Design and Analysis of Battery Thermal Management System Using Phase Change Material for Lithium-Ion Batteries in Electric Vehicles

***Muaaz Tousif., Muhammad Tahir**

Department of Mechanical Engineering, University of Engineering and Technology Lahore

DOI: https://doi.org/10.51584/IJRIAS.2025.10060023

Received: 28 May 2025; Accepted: 31 May 2025; Published: 30 June 2025

ABSTRACT

Battery thermal management system (BTMS) plays an imperative role in keeping the temperature ofbatteries in electric vehicles below 35°C to avoid power degradation and thermal runaway. The BTMS using phase change material (PCM) has advantages over other cooling techniques. It provides more cooling capacity than air cooling, more compact and less expensive than liquid cooling, more battery surface contact than heat pipes and temperature uniformity during phase change of PCM. However, it has disadvantage of low thermal conductivity. Many studies recommended the addition of fins and additives to increase heat transfer in PCM but generate the need to design a PCM BTMS for whole battery pack while considering these improvementswhich is the sole purpose of this study. The simulation of battery pack of 25 Samsung INR18650 lithium-ion cells under full discharging at 3C rate is conducted which shows temperature decreases from55°C to 36°C using commercially available paraffin PCM with 0.2 W/mK thermal conductivity.Circular fins are the most appropriate fins in battery pack and decrease the temperature to 35°C. Using PCM with expanded graphite additive decreases temperature to 33°C. It shows thatthermal conductivity enhanced by additives has more effect on PCM performance than fins andeffect of increasing thermal conductivity on decreasing maximum temperature reduces exponentially.

Keywords: Battery thermal management system, lithium ion-batteries, phase change materials, electric vehicles.

INTRODUCTION

The world's growing population and increasing standard of living, there is a growth in global energy demand. Energy consumption is rising along with technological advancement, and fossil fuels accounts for over 80% of energy [1]. Energy derived from fossil fuels has several downsides. The burning of fossil fuels results in global warming that, in turn, causes a worldwide climate disaster. As a result, it contributes to air pollution, which has been shown to have harmful effects on human health and reduce the quality of life. This long-utilized energy source has several negative side effects, including the fact that it is becoming increasingly polluted and so losing its usefulness, prompting a focus on cleaner, more sustainable options. Renewable energy sources are viable options because they are non-depletable and harmless to the environment. The primary goal should be to lessen reliance on fossil fuels and more heavily incorporate renewables into the overall energy mix.

Vehicles powered by internal combustion engines are the primary source of pollution caused by burning fossil fuels. Internal combustion engine vehicles are losing popularity to electric and hybrid electric vehicles due to fossil fuel depletion, energy problems, and climate change. Batteries are the energy source for electric vehicles, while a combination of petrol and batteries powers hybrid electric vehicles. There is a wide variety of batteries on the market, each with its capacity, lifespan, and price tag. Batteries for electric vehicles are chosen based on their power and energy densities. Because of their high specific energy and specific power, lithium-ion batteries have found widespread application. [2]

Continuous charging and discharging of battery pack in electric vehicles produces a great deal of heat. The batteries are harmed by the extreme heat that results. Batteries' efficiency and lifespan are both diminished, and new safety concerns are introduced. A battery thermal management system (BTMS) is utilized to lower and regulate battery temperatures. In other words, BTMS makes batteries more effective and trustworthy. There are three primary BTMS types. BTMS might be passive, active or hybrid. Using active cooling, like forced air or

ISSN No. 2454-6194 | DOI: 10.51584/IJRIAS |Volume X Issue VI June 2025

liquid cooling, is a part of active BTMS. In passive BTMS, heat pipes or phase change material PCM are used to control temperature. Hybrid BTMS include those that combine PCM with air, liquid or heat pipe. The latent heat is absorbed by the phase change material PCM. Large sensible and latent heat, a high k value, low density, cost-effectiveness, non-reactant with the anode, cathode, and electrolyte of battery, thermal stability, and availability are all hallmarks of a high-quality PCM. [3]

Internal combustion engine vehicles contribute to air pollution and global warming. Three-quarters of the pollution caused by transportation comes from public transportation. Most of this comes from cars and buses, which account for 45.1% of it. Three-quarters of the pollution caused by transportation comes from public transportation. Most of this comes from cars and buses, which account for 45.1% of it. Cargo trucks account for the remaining 29.4% [4]. The development of EVs and HEVs has become a critical concern for the future due to the depletion of the world's oil reserves along with efforts to reduce carbon dioxide. Due to increased environmental awareness and the utilization of sustainable energy sources to combat global warming, the electric car market share is rising. The life cycle reports demonstrate that internal combustion engine vehicles have negative impacts on the environment and human health in particular. Increased use of EVs may also reduce air pollution, noise pollution, and pollutant intensities, ultimately improving the local air quality. Fuel costs and environmental effects for operating EVs, HEVs (Hybrid Electric Vehicles), and PHEVs (Plug-In Hybrid Electric Vehicles) are significantly lower than for internal combustion engine vehicles. The electric vehicles (EVs) development is regarded a vital element in the battle against global warming and the reduction of vehicular pollution. Electric vehicles obtain their power from batteries. The market of EVs and HEVs is increasing at a high rate. Based on the forecast, these their market will be 46.2% in 2020 and 60.2% in 2030 [5]. New electric vehicles (NEVs) market prediction trend is represented in Fig. 1 which predicts the dominance of EVs and HEVs in the future.

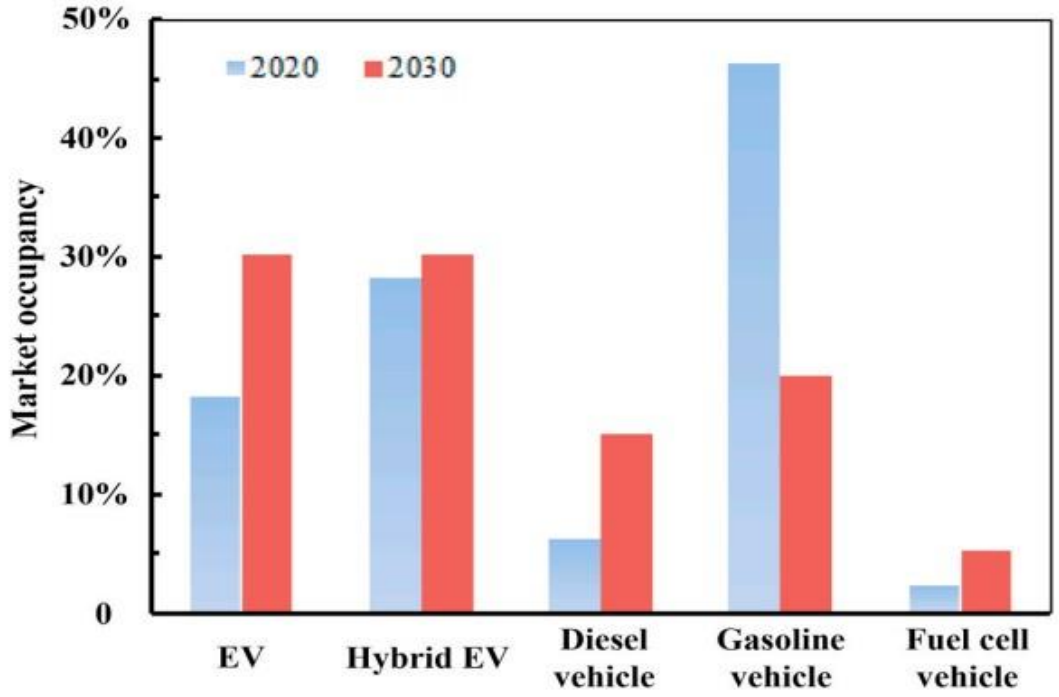

Figure 1 Market occupancy prediction [5]

The battery provides energy to the induction motor, which drives the gearbox and then the wheels of the EV. Significant breakthroughs such as the improvements in battery system may be made in in electric vehicles. The gravimetric energy density (the available energy per unit mass of a substance) is the most significant factor when choosing batteries [6]. Lithium-ion batteries (LIBs), which offer a high energy density, a low self-discharge rate, a long cycle life, and no memory effect, have replaced conventional batteries as the go-to power source for NEVs. Li-ion batteries not only have a remarkable energy density, but also a superior power density in comparison to other rechargeable batteries [7]. China is currently the largest EV market in the world, and by 2030, it is predicted that China's demand for LIBs for EVs will reach 740 GWh [8]. Ragone plot indicates that

ISSN No. 2454-6194 | DOI: 10.51584/IJRIAS |Volume X Issue VI June 2025

Lithium-ion batteries possess high specific energy as well as high specific power as compared to other batteries Fig 2 [7]. Lithium-ion batteries are commonly used in EVs as energy sources. The performance and durability of the batteries used in electric vehicles are crucial components for ensuring buyer confidence.

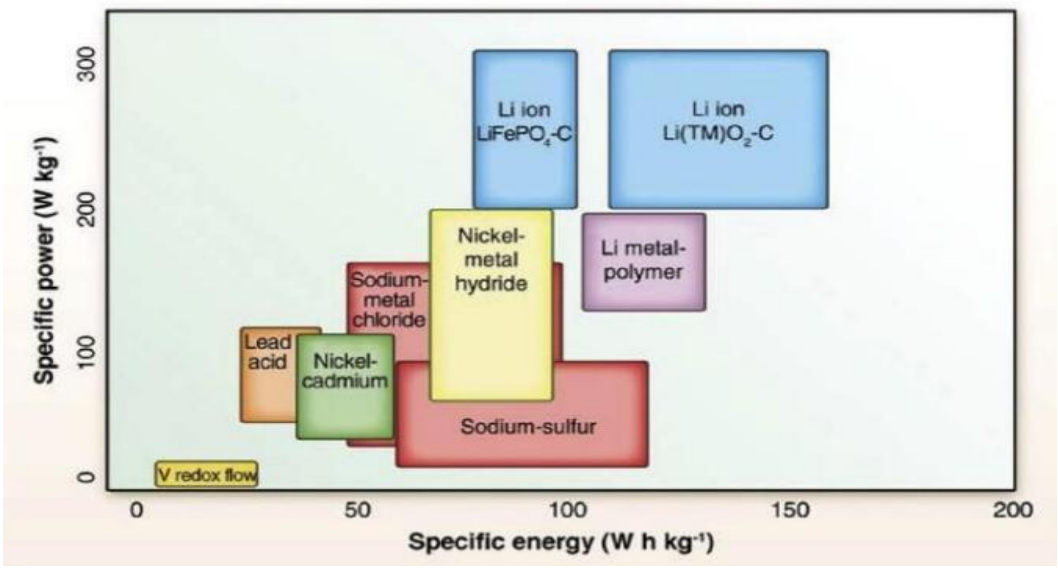

Figure 2 Ragone plot for different batteries [7]

Generally, there are two types of Li-ion battery models: empirical models and electrochemical models. These models are used to find the State of Health (SOH) and State of Charge (SOC) of battery. The empirical models depend on the experimental history of the battery [7]. Empirical models' key benefits are they are quick and straightforward in terms of computation. They do, however, have some drawbacks. For instance, it is impossible to identify the physics-based parameters. A battery's properties are never updated as it gets older, hence the empirical model of one battery type cannot be used for another. As a result, after a given charge/discharge cycle, battery management systems using empirical models do not function effectively which necessitates the use of sophisticated electrochemical models [7].

In EVs and HEVs, battery charging and discharging generate a lot of heat. The power packs must release heat rapidly to the surrounding environment to avoid overheating (caused by heat created inside the cells). The temperature has impact on different parameters of battery. It not only affects the charge and discharge efficiency, energy capacity and power output of batteries but also have an impact on lifespan and safety of batteries [9]. The heat produced by the charging and discharging processes causes the battery pack temperature to rise. Depending on the charge/discharge rate (C-rate), different amounts of heat are produced As a result, the battery's capacity declines, its state of charge (SOC) drops, it ages, it breaks, it explodes, and it may even catch fire. Because Li-ion batteries' performance, lifespan, and safety are reliant on temperature, the highest temperature of the battery (Tmax) and the highest temperature difference between the cells (ΔTmax) are considered [10]. The required maximum temperature and its differential of lithium-ion batteries for an effective BTMS is within 15°C to 35°C and 5°C respectively [10].

The battery system needs thermal control to prevent thermal runaways and maintain performance. The battery can avoid capacity loss and lifespan reduction by being maintained within a specific temperature range. A substantial amount of heat is produced as the batteries are rigorously charged and discharged. Consequently, a capable BTMS is required to control an EV battery's working environment.

Calculation of internal heat generation in batteries is a complex concept because it depends on the state of charge, current, internal resistance, initial temperature, and C-rate. Calculation of heat generation can be performed through various methods. While neglecting reversible heat generation only, Irreversible heat generation calculations are widely used to avoid complexity [11]. Temperature variation in a cell can create a local hot site. Such heated spots would induce internal short circuits, which, under some severe situations, may cause a fire or an explosion. Additionally, changes in internal cell temperature would affect chemical reaction rates, which

ISSN No. 2454-6194 | DOI: 10.51584/IJRIAS |Volume X Issue VI June 2025

would become more prominent with an increase in the number of cycles [12]. A battery pack consists of several cell connected in parallel or series in order to meet varying voltage and power requirements. Temperature changes have a considerable impact on battery packs performance. Maintaining a suitable temperature range is essential for avoiding power degradation and thermal runaway. The excessive heat causes the thermal runaway which further increases the heat and becomes a fire hazard. When an internal cell dies, its energy quickly travels to nearby cells, interrupting the power available for discharging and charging [6]. In order to resolve all these disadvantages and hazards of high temperature, a competent battery thermal management system (BTMS) is required to govern the working environment of an EV battery.

Comparison of BTMSs

Several battery BTMSs have been developed which includes air, liquid, heat pipe (HP), and PCM based BTMSs [13]. The air-based BTMS is the first kind of BTMS; it is also the simplest to implement, the lightest in weight, and the least expensive both to purchase and maintain which is installed in EVs such as Nissan Leaf, Mitsubishi i-MiEV and Audi Q5 [14]. Low cooling efficiency and capacity are its main drawbacks. This means that modern high power electric vehicles which generates a lot of heat cannot be cooled by BTMSs that rely on air [15]. BTMS with liquid cooling offers greater efficiency of cooling as well as higher cooling capacity than air-based BTMS [16], so it is installed in new EVs such as Tesla Model S, BMW i3 and i8, Chevrolet Volt, and Audi Q7. Liquid-based BTMS has the drawback of leaks and requires additional pipes and pumps, which raises the system's overall size, complexity, and expense [17]. These active cooling BTMS also cause an uneven distribution of temperatures across the battery pack when the discharge rate is high. Due to these issues, research into passive cooling BTMs using heat pipes and phase change materials has been a priority (PCM). While heat pipes' high thermal conductivity helps speed up heat transfer at high discharge rates, good surface contact between battery cells and the pipes is crucial to their effectiveness as a BTMS.

PCM-based BTMS, on the other hand, can cool batteries more effectively than air-based BTMS. It is more compact than liquid-based BTMS, and may be used with batteries of a larger variety of geometries than heat pipes [18]. Additionally, it offers benefits including reduced energy usage, low price, and great temperature consistency [19], [20].

Nevertheless, there are two limitations of PCM-BTMS [21]. One is the low heat transfer rate Q in pure PCM, such as paraffin, due to its very low thermal conductivity. Having a low Q means that PCMs will not absorb heat from the battery as quickly, which will cause $T_{battery}$ to rise more quickly [22]. The second one is the limited latent heat H_{PCM} that can be absorbed by PCM [23]. The PCM control temperature while it is melting. Limited H_{PCM} will cause the PCM to melt completely after absorbing specific amount of heat which in turn do not control the temperature anymore [22]. The risk of thermal runaway is increased because molten PCM acts as thermal insulation between the batteries and the heat sink. Solutions for these issues include increasing the PCM's heat transfer rate Q and coupling the PCM with other cooling technologies to recover H_{PCM}.

Heat transfer enhancement

The rate of heat transfer (Q) between the battery and the PCM, which is in direct contact with the battery, is described by the equation:

$$Q = hA(T_{battery} - T_{pcm}) \quad (1)$$

Where h is the heat transfer coefficient, A is the surface area between the battery and PCM, $T_{battery}$ is the battery temperature and T_{pcm} is the PCM temperature. According to Eq. (1), Q can be improved by increasing h and A or decreasing T_{pcm}. Decreasing T_{pcm} would be impractical as the temperature of PCM should be enough for it to melt and take advantage of latent heat and temperature uniformity. Since the contact and battery side thermal resistance are so much smaller in comparison to the PCM side thermal resistance, h is the reciprocal of the total thermal resistance, which is the sum of the PCM side thermal resistance, the battery side thermal resistance, and the contact thermal resistance. Thus, lowering the PCM side's thermal resistance, achieved by increasing the PCM's thermal conductivity, will raise h and thus raise Q. Multiple fin arrangements are used to achieve the same goal (an increase in A).

ISSN No. 2454-6194 | DOI: 10.51584/IJRIAS |Volume X Issue VI June 2025

Increasing Heat transfer coefficient

The thermal conductivity of PCM can be increased by adding metal meshes, porous media, and Nano-material additives in PCM. Metal meshes are usually of aluminum and copper. Porous media include nickel foam, copper foam, aluminum foam, and expanded graphite. Nano-material additives include graphene and carbon nanotubes.

Wang et al. [24] added aluminum foam which increased the PCM thermal conductivity by 218 times. It resulted in the maximum rise in temperature decreased by 20% compared to pure paraffin under a 2C discharge rate. Further study by Alipanah and Li. [25] showed that thermal conductivity rises when the porosity of aluminum foam in PCM decreases. Reducing the porosity of aluminum foam from 0.97 to 0.88 raised its thermal conductivity from 6 to 25 W/(mK). The temperature between batteries was negligible by adding aluminum foam.

Hussain et al. [26] used the nickel foam in paraffin which increased its thermal conductivity by 4.8 times compared to pure paraffin PCM. Hussain et al. [27] then used the graphene-coated nickel foam to further increase thermal conductivity which was 22 times as compared to only nickel foam. It resulted in the rise temperature of the battery being 17% lower than paraffin with nickel foam.

PCM with paraffin-filled copper foam was investigated by Mehrabi-Kermani et al. [28]. Thermal conductivity was increased by more than 40 times. He et al. [29] added expanded graphite in copper foam which further increased thermal conductivity by an increment of 7 times.

PCMs with copper micro fibrous were studied by Zhu et al. [30]. It was found that Copper micro fibrous increases the thermal conductivity by approximately 275 times. This large enhancement resulted in the battery maximum temperature always being maintained below 48 °C, which is much less than the threshold temperature of 60 °C, even when the discharge rate is as high as 15C. The expanded graphite was used by Jiang et al. [31]. Thermal conductivity is increased by 69 times for 30% mass fraction of expanded graphite. Increasing mass fraction linearly increases thermal conductivity however it also decreases the latent heat of PCM. However, LPCM decreased simultaneously. Consequently, a mass fraction of 9–20 wt. % expanded graphite is recommended for optimum thermal management performance.

Azizi and Sadrameli [32] investigated the performance of PCM-BTMSs with aluminum mesh.

The increased thermal conductivity increases battery temperature distribution uniformity, while 1C and 3C discharge rates lower maximum battery temperature by 19% and 26%, respectively. Situ et al. [33] compared the performance of single and double copper mesh with expanded graphite. Thermal conductivity for double copper mesh was 11.2 times which was higher than 8 times for expanded graphite and 9.4 times for single copper mesh.

Karimi et al. [34] used copper nanotubes and found the enhancement of thermal conductivity by only 2.5 times. It can be increased by using graphene and expanded graphite with copper nanotubes to increase thermal conductivity by 12.4 times as proposed by Zou et al. [35].

In summary, copper micro fibrous provides the maximum thermal conductivity enhancement of 275 times to PCM. In porous additives, the aluminum foam has the greatest thermal conductivity improvement, which is more than 166 times [36]. Then comes the copper foam and then nickel foam of only 4.8 times. Expanded graphite is also widely being used having enhancement ranging from 3.3 [37] to 69 times depending upon mass fraction. The enhancement offered by nanomaterial additives are significantly lower than porous foams.

Increasing heat transfer area

Ping et al. [38] studied the performance of PCM-fin BTMS and then compared it with pure PCM and PCM with expanded graphite. Even at 3C discharge rate, the use of longitudinal fins incorporated in PCM may control the maximum battery temperature below 51°C. The comparison, based on maximum battery temperature against time, is presented in Fig. 1. Fins not only increase the heat conduction but, unlike expanded graphite-filled PCM, also improve natural convection so they have better performance.

ISSN No. 2454-6194 | DOI: 10.51584/IJRIAS |Volume X Issue VI June 2025

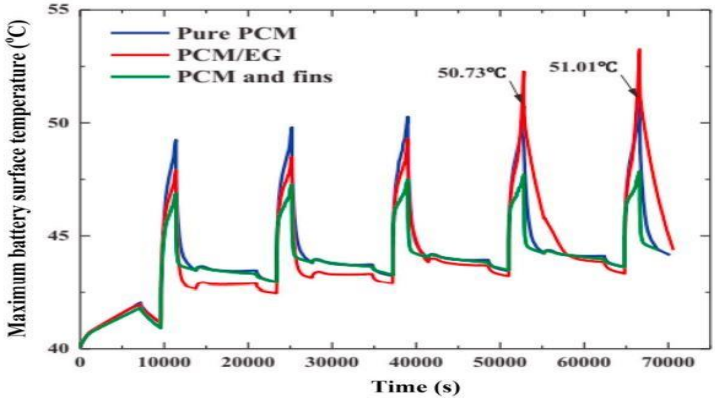

Figure 3 Graph of maximum battery surface temperature with time for BTMSs with PCM-fin structure, expanded graphite-filled PCM, and pure PCM [38].

Wang et al. [39] analyzed how 8 fins in a PCM framework may boost heat transmission by 170%.

The results showed that even at a discharge rate of 5C, the battery temperature could be kept below 50 degrees Celsius. Sun et al. [40] proposed a design for a PCM-fin structure, which can be seen in Fig. 2, and claimed that it would increase the area by linking all of the fins with cylinder rings. Because of the performance improvement, the temperature of the battery can be managed, even when it is being discharged at a rapid rate, Zheng et al. [41] analyzed the effect of fin parameters and suggested 8 aluminum alloy fins with the length of 7.5 mm and 0.5 mm thickness for optimal performance. When comparing the PCM-fin structure to pure PCM, 60% increase in duration time for effective operation of battery was found.

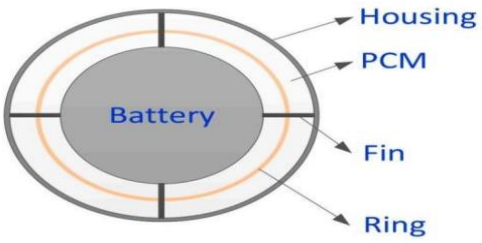

Figure 4 Schematic of cylindrical rings within PCM with fins [40]

Weng et al. [42] proposed different fin configurations namely X-shaped, Y-shaped, and V-shaped fins as shown in fig. 3 and then compared their performance with rectangular fins. The maximum battery temperature in case of pure PCM without fins was found to be 52 °C while for rectangular fins it was 50°C. For V-shaped fins, it was 48.5°C and for the fins shaped in Y, it was 47.0°C.

Finally, the fins shaped in X structure had maximum battery temperature of 46.9°C. It showed that the fins of X shape provided better thermal management performance compared to others. It is because X-shaped fins provide more heat transfer area.

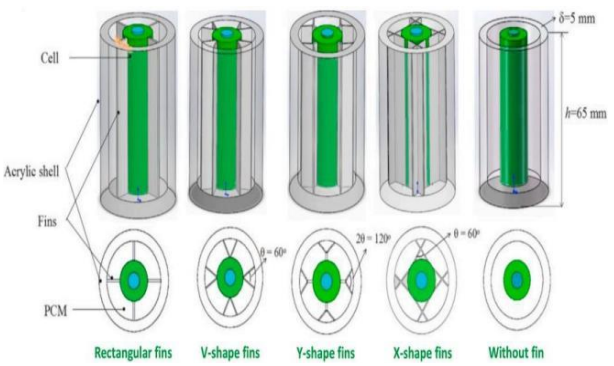

Figure 5 Fins configuration presented by Weng et al. [42]

ISSN No. 2454-6194 | DOI: 10.51584/IJRIAS |Volume X Issue VI June 2025

Choudhari et al. [43] studied fin shape, fin number, PCM thickness, and convective coefficient at PCM housing and analyzed their effect on discharge rates. Specifically, it was suggested that a battery module be optimized with I-shaped fins, convective coefficient of 15 W/(m2 K), fin number of 4, and PCM thickness of 26 mm. At a discharge rate of 3C, the results showed that the use of fins decreased the batteries maximum temperature by 6.4 K and the temperature difference by 1.58 K. As a result, it was determined that fin form has a minimal impact on battery temperature.

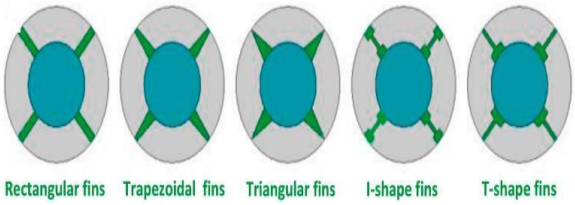

Figure 6 Different fin shapes studied by Choudhari et al. [43].

Coupled PCM-BTMS

PCM is coupled with air cooling, liquid cooling, heat pipe (HP) cooling, or thermoelectric (TE) cooling to recover the thermal storage or latent heat capacity H_{PCM}. Other cooling methods include air cooling. These coupling strategies were reviewed by Shen et al. [5] and shown in fig. 5.

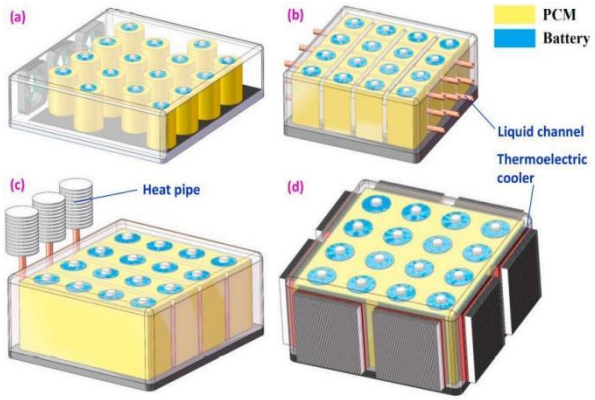

Figure 7 Coupled BTMSs having PCM with: (a) forced air cooling, (b) liquid cooling, (c) heat pipe cooling and (d) thermoelectric cooling [5]

Maximum temperatures of 46 °C was measured with ambient temperature of 34 °C and discharge rate of 2 C and an while testing the effectiveness of forced air conditioning paired BTMSs [5]. PCM and air coupled BTMS has numerous advantages namely low weight, cost, and maintainability, but it requires improvement in their thermal performance at high temperatures under large discharge rates [44].

Thermoelectric coolers (TECs) are solid-state devices that use the principle of thermoelectric effects in semiconductors to cool down the surrounding air. To keep PCM within an acceptable temperature range, TEC can either cool it or heat it, depending on the surrounding temperature. Despite their potential, TECs have a limited scope of use because of their low efficiency and short lifespan [44].

Considering the importance of surface contact on the effectiveness of the heat pipe, the design of BTMSs with PCM and heat pipe was presented as shown in fig. 5 (c) [5]. The PCMs' evaporator sections were installed vertically within the PCMs, while the condenser sections were located externally and cooled using air or liquid. Experiments showed that at a discharge rate of 5C and 3 m/s air velocity over the condenser portion, batteries maximum temperature stayed below 50°C, extending their effective operating time by 10% compared to when they were not equipped with heat pipes. While the addition of a heat pipe with a very high heat transfer rate can help avoid PCM overheating, this passive HP-linked PCM-BTMS may not be enough for some applications, especially those with extremely high discharge rate demands [44]. In coupled PCM-liquid BTMS, liquid-cooled tubes and cold plates are used in PCM to exchange the heat from PCM to flowing liquid in mini channels as

ISSN No. 2454-6194 | DOI: 10.51584/IJRIAS |Volume X Issue VI June 2025

represented in fig. 5 (b) [5]. A PCM and liquid coupled cooling system appears to be an efficient option, as the PCM keeps the battery within its optimal operating temperature range and the liquid cooling, with its high cooling capacity, efficiently recovers the PCM latent heat. One parameter that allows efficient and economical temperature regulation across an entire PCM is its latent heat. Achieving the same level of performance with a BTMS that relies solely on liquid cooling could be more expensive and time-consuming to design [44].

Battery thermal modeling

Battery thermal models are classified into three types which vary according to the amount of knowledge necessary to explain the model. These are white, grey, or black-box model as described by W. Allafi et al. [45]. Experimentally determined characteristics and physical attributes of the system are used to build the white-box model. Electrochemical-thermal models of one, two, or three dimensions are examples of white-box thermal models. In contrast, the black-box model requires small knowledge about the physical principles governing the battery. The practical importance of model parameters, such as thermal capacity and conductivity, is lost in this model.

The grey-box model incorporates the lumped-parameter (LP) model.

Lumped thermal model

Lumped model is fast and can be implemented easily so it is considered the most efficient model for thermal management. It is derived through physical knowledge of the system and model parameters estimated from test data. This model shows extremely close agreement with experiments at Biot numbers less than one, and its sole downside is the departure from experimental findings at large discharge rates [46]. In the lumped thermal model, we present the battery as a single node with equivalent physical properties so it ignores batteries temperature distribution which becomes the problem at high-temperature gradients. More complicated 2D or 3D electrochemical thermal models are used in this case.

W. Allafi et al. [45] offered a description of a simple heat transfer model with lumped parameters.

For a battery, the balance of heat addition and release satisfying energy conservation is stated as:

$$(dT(t)/dt) = Q_{ge}(t) - Q_{loss}(t) \quad (2)$$

Which gives the solution for cell temperature, with time. Here, $Q_g(t)$ is the rate of battery heat generation and $c = \rho C_p$ represent the thermal capacity of battery. C_p is the specific heat of battery and ρ is the cell density. $Q_{lo}(t)$ represents the heat loss from battery to the surrounding environment. It has two parts namely convective and radiative heat loss. The convective heat loss is described as:

$$(t) = hA(T(t) - T_{amb}(t) \quad (3)$$

Where h is the convective heat transfer coefficient, $T_a(t)$ represent ambient temperature and A is the area. Using Stefan-Boltzmann law, the radiative heat transfer is represented as:

$$(t) = \sigma A(T^4(t) - T_{amb}{}^4)(t) \quad (4)$$

Where ε and σ are the emissivity and Stefan–Boltzmann constant respectively.

Two or three-dimensional Electrochemical-thermal models

These models have excellent agreement with experiments and provide significant information for analyzing the batteries but they are time-consuming, complex, and require high computational costs [46]. These models consider the temperature distribution and temperature gradients in cells and their effects at high discharge rates [46].

ISSN No. 2454-6194 | DOI: 10.51584/IJRIAS |Volume X Issue VI June 2025

Heat generation modeling

Heat generated by the battery Q_{gen} is required in equation (2) for complete thermal modeling of the battery. Undercharging/discharging operation of lithium-ion batteries, there are 4 sources of heat generation: resistive or joule heating (irreversible term), the entropy of cell reaction (reversible term), heat of mixing, and side reactions [45]. There are 3 heat generation models depending upon the heat sources they consider. These are Maximum constant power, Reversible and irreversible term, and Electrochemistry heat generation models.

Maximum constant power

The most basic model assumes that the rate of heat generation from the battery remains constant at any given discharge rate; moreover, this rate is assumed to be at its highest possible value for this model. The only place where it can be used is in the analysis of cooling systems, where its conservative approach to cooling design and subsequent overdesign of cooling systems proves to be quite helpful [46]. The constant heat generation rate is usually found from experiments and given in literature at different discharge rates.

Reversible and irreversible term

This heat generation model considers the irreversible resistive or ohmic term and reversible entropy term of heat generation. This model's compatibility with lumped thermal model and the electrochemical-thermal model makes it popular among scientists. This model is straightforward, quick, and provide agreement with the experiment for low and average discharge rates, but it deviates at high discharge rates since it does not account for all battery phenomena [46]. The equation for heat generation per unit volume of battery q_{gen} is developed by Bernardi et al. as:

$$q_{gen} = \frac{}{V_{bat}} I\left((E_{OCV} - V) - T \frac{d}{dT} E_{OCV}\right) \quad (5)$$

Where irreversible heat is represented by first term and reversible heat by second term. E_{OCV} is open circuit voltage, I is current and V is voltage across battery terminals. E_{OCV} is a function of the state of charge. V_{bat} represents the volume of the battery while T is the temperature of the battery [45].

Electrochemistry model (P2D)

Electrochemistry models consider the electrochemistry of batteries and thus provide a more precise estimate of heat production, which is required for constructing an effective cooling system. Pseudo-two-dimensional P2D and single-particle model are the two most common dimensional electrochemical models. The P2D model relies on the porous electrode theory, the kinetics equations, and the concentrated solution theory [7]. The results of this model are validated against experiments from low to high discharge rates and the disadvantage of the P2D model is complex and time consumption [46].

The single particle model SPM is a simplification of Pseudo-two-dimensional model P2D to decrease its lengthy calculation times. Transport phenomena are simplified and the electrolyte is disregarded in SPM. However, temperature circumstances' impacts on the performance of batteries are considered [7].

Research Gap

Many researchers have studied and compared the performance of different kinds of PCM-BTMS. As described earlier, they have studied the improvements in PCM by adding meshes, porous media, and other Nano-material additives. Some of them have investigated the impact of adding fins on BTMS performance. while many of them have studied the coupling of different cooling methods with PCM. What we have found missing, or a research gap, is the use of the improvements of PCM material additives, fins, and couplings together in a single coupled PCM-BTMS. The reason for this is that they studied these improvements in very great detail which leaves no room to incorporate other improvements. On the other hand, we use the results of their studies on different improvements together in our design.

ISSN No. 2454-6194 | DOI: 10.51584/IJRIAS |Volume X Issue VI June 2025

MATERIALS AND METHODS

Physical Model, Governing Equations and Boundary Conditions

The schematic of physical model is shown in Fig. 8. The batteries indicated with red are enclosed inside the PCM block with height H of 65 mm and width W and length L of 134 mm. The battery model is 18650 with dimensions of 18 mm diameter and 65 mm height. The detailed description of battery used in our analysis is shown in Table 1. The PCM used is the commercially available organic paraffin PCM with properties described with detail in Table 2.

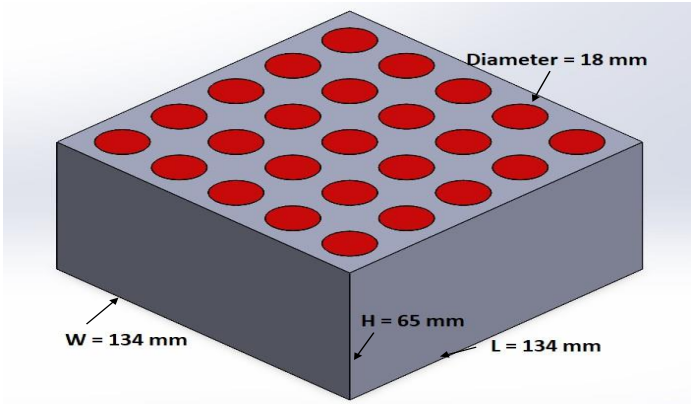

Figure 8 PCM model dimensions

Table 1: Properties of battery used [10]

Property	Unit	Value/Specification
Chemical abbreviation	-	NMC
Cathode material	-	LiNiMnCoO2
Anode material	-	Carbon
Density ρ	Kg/m3	2775
Specific heat Cp	J/kgK	880
Thermal conductivity	KW/mK	Axial=30 [c-p] Radial=0.8
Internal resistance Ri	mΩ	20
Diameter D	mm	18
Height H	mm	65
Nominal Capacity	mAh	3000
Maximum voltage	V	4.2
Nominal voltage	V	3.6

Table 2: Properties of commercially available paraffin PCM

Producer	Plus Advanced Technologies
Model	OM32
Type	Organic PCM

ISSN No. 2454-6194 | DOI: 10.51584/IJRIAS |Volume X Issue VI June 2025

Phase transition temperature ('C)	30-33
Density (kg/m3)	926
Specific Heat (kJ/kg K)	3.21
Latent heat (kJ/kg)	187
Thermal conductivity (W/mK)	0.219

The batteries will act as the continuous heat source and PCM will act as heat sink as shown in Fig. 9. The battery will generate heat at the rate of P = 1 04017 W/m^2 at 9 Ampere current and 3 Coulomb discharge rate. The three-dimensional (3D) heat transfer analysis is considered involving conduction of heat between batteries and PCM. The PCM walls are considered insulated.

The above-mentioned physical model is described by governing equation of three dimensional (3D) heat transfer equation:

$$\frac{\delta}{\delta x}\left(k\,\frac{\delta T}{\delta x}\right)+\frac{\delta}{\delta y}\left(k\,\frac{\delta T}{\delta y}\right)+\frac{\delta}{\delta z}\left(k\,\frac{\delta T}{\delta z}\right)+q^{v}=\rho c_{p}\frac{\delta T}{\delta t}$$

Where k is the thermal conductivity already known. q_v is the rate of heat generation per unit volume, $_p$ is specific heat capacity and ρ is the density.

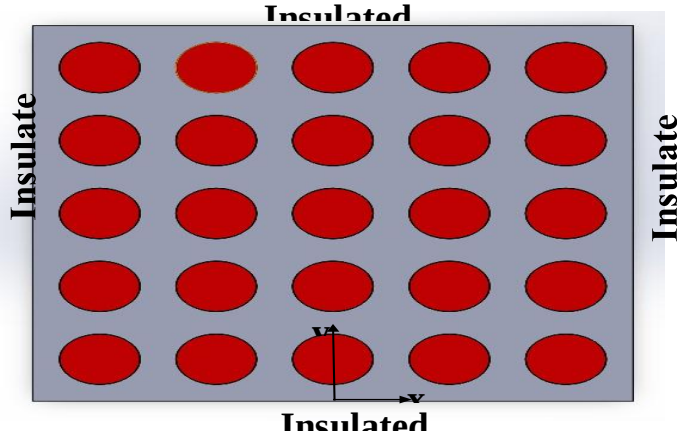

Figure 9 Battery as heat source

For this static system with no displacement in any direction i.e. u, v, w = zero, the momentum equation and continuity equation are not the governing equations. The boundary conditions for above heat transfer equation are:

1) Adiabatic boundary condition at left and right PCM wall

$$\frac{\delta T_{PCM}}{\delta x}=0 \quad at\ x=\frac{W}{2}\ \frac{-W}{2},$$

2) Adiabatic boundary condition at front and back PCM wall

ISSN No. 2454-6194 | DOI: 10.51584/IJRIAS |Volume X Issue VI June 2025

$$\frac{\delta T_{PCM}}{\delta y} = 0 \quad at\ y = -\frac{L}{2}, \frac{L}{2}$$

Heat generation boundary condition

$qv,battery = P$

Where P = 104017 W/m^2, given in literature [10].

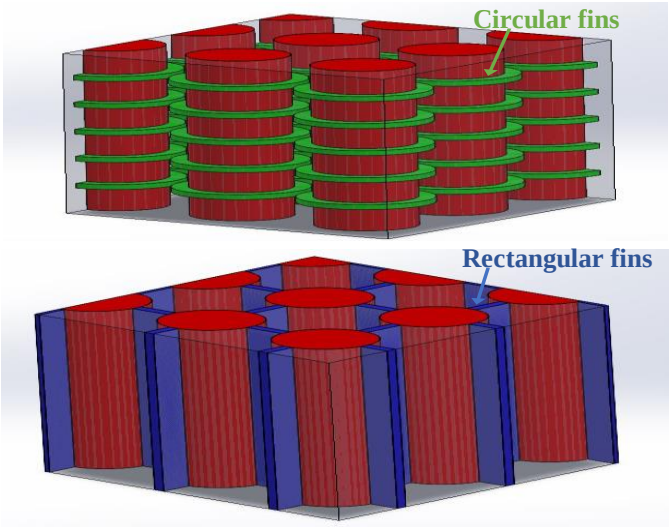

Figure 10 PCM model with Circular fins and Rectangular fins

The models with rectangular and circular fins and one another model having additives inside the PCM follow the same energy equation of heat transfer. The fins used are made up of aluminum while the additive is expanded graphite.

Analysis Procedure and Characteristics

The analysis procedure for this study involved examining five distinct cases, as presented in Fig. 11. In the first case, batteries maximum temperature was determined without any cooling mechanisms, serving as a baseline for comparison. The second case involved incorporating paraffin PCM to gauge its impact on the system's temperature. The third case entailed the insertion of various types of fins to enhance the model's performance. In the fourth case, additives like expanded graphite were introduced to compare their effectiveness with fins. Table 4 showcases the properties of PCM with expanded graphite. Lastly, the fifth and final case integrated both fins and additives, with their collective performance evaluated. All these cases are simulated under discharge rate of 3C for 1200 seconds.

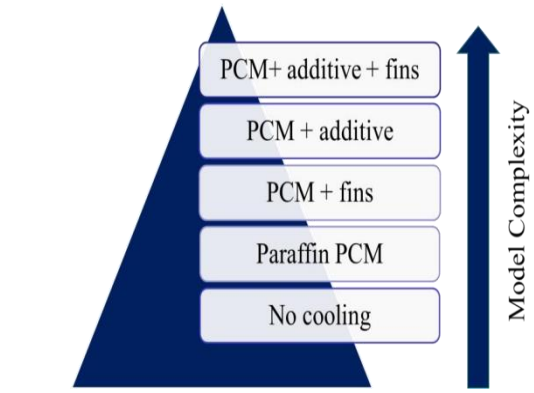

Figure 11 Cases Simulated

ISSN No. 2454-6194 | DOI: 10.51584/IJRIAS |Volume X Issue VI June 2025

The anisotropic thermal conductivity of cylindrical battery is used in order to better represent the battery. Due to different structure in different directions, the radial thermal conductivity, perpendicular to the layers of sheets in battery, is very small compared to the tangential or axial thermal conductivity which is along the layers.

Table 3: Properties of PCM with expanded graphite [44]

Phase transition temperature ('C)	30-33
Density (kg/m3)	870
Specific Heat (kJ/kg K)	2.412
Latent heat (kJ/kg)	119.24
Thermal conductivity (W/mK)	5.023

Due to the complexity and time-consuming nature of simulating the phase change material with all the fins inserted into the model, a simplified approach was implemented. Specifically, a quarter of the geometry was analyzed with symmetry applied to the inner two faces. This not only simplified the analysis but also enabled us to visualize the temperature distribution within the middle cross-section of the model.

One of the key boundary conditions in solving the energy equation is about battery's heat generating rate. To ensure simplicity in our analysis, a constant heat generation rate was utilized, with values per unit volume of the battery determined from literature [10] and presented for different values of discharge rate C in Table 3.

To ensure that our model correctly simulate the heat generation, the heat generation rate at a specific discharge rate is used from this table and then batteries are simulated without any phase change material. The resulting temperature of batteries is compared with experimental results from another literature source and the error is found.

Table 4: Rate of heat generation at different discharge rates by [10]

Parameter			Values		
Discharge rate (C-rate)	1	2	3	4	5
Battery Current (A)	3	6	9	12	15
Rate of heat generation (W/m3)	12907	47579	104017	182220	282189

Numerical Method and Mesh

Numerical simulations of fluid dynamics were conducted using the commercial software FLUENT 21.0. The computational domain was discretized using a second order scheme, and the resulting equations were solved using the finite volume method. To determine the corrected pressure and velocity components, the widely-used SIMPLE algorithm was employed. The convergence of the solutions was assessed by ensuring that all calculated parameter residuals were less than 10^-6. The under-relaxation factors for the continuity, momentum, and energy equations were set to 0.3, 0.7, and 1.0, respectively. In FLUENT, 'Solidification and Melting' module is used along with energy equation for the effective simulation of phase change material (PCM) temperature, phase transition and liquid fraction. 'Solidification and Melting' module require phase change temperature along with other PCM properties provided in Table 2 and Table 4.

In order to generate accurate results for all the models being analyzed, a consistent meshing method was utilized. Specifically, the Sweep method with Quad/Tri mesh type and program-controlled algorithm was used throughout the simulations. Additionally, Sweep was applied specifically to improve the mesh for the battery's circular geometry. The edges were also sized with 20 divisions to ensure proper resolution. The resulting mesh quality

ISSN No. 2454-6194 | DOI: 10.51584/IJRIAS |Volume X Issue VI June 2025

was evaluated, and it was found that the minimum average mesh quality for circular fins was 0.82, as illustrated in Fig. 12.

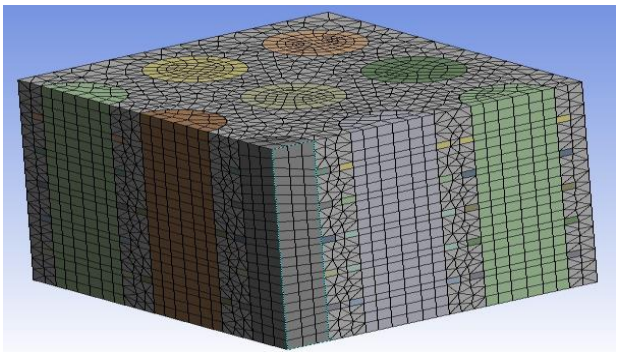

Figure 12 Mesh shown at inner cross section in case of circular fins

RESULTS AND DISCUSSIONS

In this chapter, we present the simulation results for different cases of battery cooling using various methods. Before discussing the results, we first validated our model's accuracy in simulating heat generation by comparing the simulated results without any cooling mechanism to experimental data from literature. The validation was done using a specific discharge rate, and the heat generation rate was obtained from literature. The resulting temperature of the batteries was compared with the experimental data, and the error was calculated. Once the model's accuracy was validated, we proceeded to study the effect of different cooling methods on battery temperature. We first examined the batteries' maximum temperature without any cooling mechanism as a baseline for comparison. Then, we analyzed the impact of incorporating a phase change material (PCM) and different types of fins and additives. Lastly, we evaluated the collective performance of both fins and additives when integrated. The simulation results and their analysis are presented in the following sections.

Heat Generation Validation

The accuracy of the model in simulating heat generation was validated by comparing the maximum temperature of batteries without any cooling mechanism, obtained from the simulation, with experimental results from literature. The simulation was done using a constant heat generation rate per unit volume of the battery, which was determined from literature. The validation was performed at a specific discharge rate, and the results are presented in Fig. 14. The graph shows the change in batteries maximum temperature with time, and both the CFD results from this study and the experimental results from literature are plotted on the same graph. The maximum error between the simulation and experimental results was found to be 5%, indicating good agreement between the two. The validation graph demonstrates that the model accurately simulates the heat generation of the batteries and can be used to investigate the effects of different cooling methods on the battery temperature.

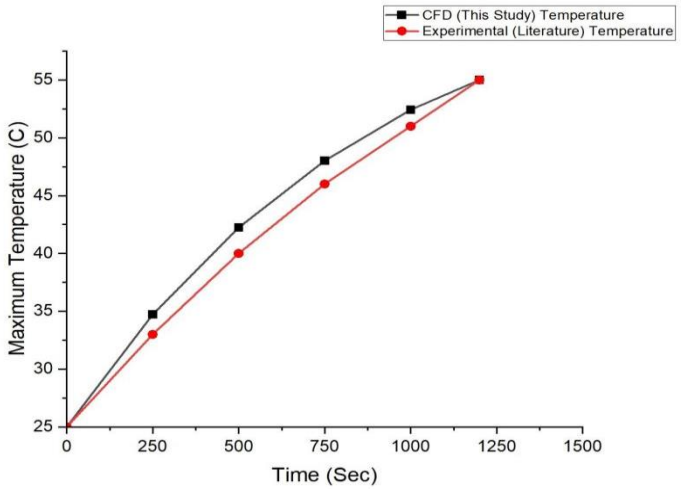

Figure 13 Heat generation validation at 3C discharge rate

ISSN No. 2454-6194 | DOI: 10.51584/IJRIAS |Volume X Issue VI June 2025

Comparison of Maximum temperature

The maximum temperature for all the cases under discharge with 3C rate for 1200 seconds is shown in Table 5. The Fig. 14 presents the maximum temperature of the batteries over time for all six cases studied. The y-axis represents batteries maximum temperature in degrees Celsius, while the x-axis represents time in seconds. The graph shows that the maximum temperature of the batteries without any cooling mechanism (case a) rises rapidly and reaches its peak value of 55 degrees Celsius within few minutes. In contrast, the use of cooling methods such as PCM, along with fins and additives, causes the maximum temperature to rise gradually, with the peak value being significantly lower than that of the 'No cooling' case. The graph also shows that the combination of additives and circular fins (case f) yields the lowest maximum temperature among all the cases studied. This maximum temperature graph provides a clear visualization of the effectiveness of different cooling techniques in reducing the maximum temperature of the batteries.

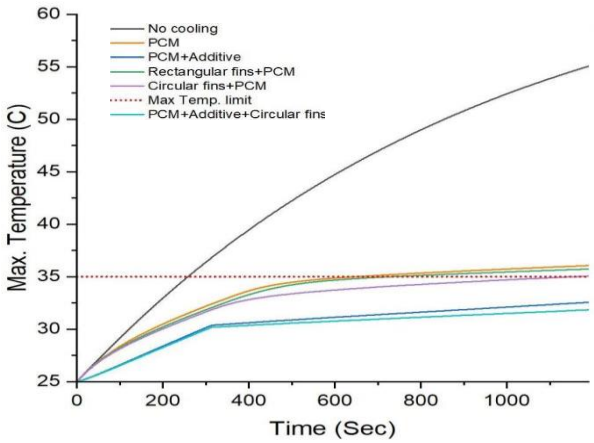

Figure 14 Rise of maximum temperature with time for different cases studied

Table 5 Maximum temperature after 1200s under 3C discharge rate for different cases

Case	Configuration	Max Temperature (°C)
a	No cooling	55
b	Paraffin PCM	36
c	PCM + Rectangular fins	~36
d	PCM + Circular fins	35
e	PCM + Additive	33
f	PCM + Additive + Circular fins	32

Temperature Distributions

Fig. 15 compares the temperature distributions of different cases on a common scale of temperature ranging from 27 to 35 degrees centigrade. The graph provides a clear visualization of the temperature distribution of each case and how it compares to the maximum allowable temperature for optimum battery performance and lifespan. The different cases are represented by different colors, making it easy to compare their temperature distributions. By analyzing the graph, it is apparent that the cases with additives and/or fins showed a considerable decrease in the temperature of batteries. The case with PCM, additives and circular fins (Case f) shows the lowest temperature distribution, indicating that the combined use of additives and circular fins is the most effective cooling method among all the cases. The graph provides crucial insights into the performance of different cooling mechanisms in managing the temperature of batteries, enabling us to identify the most effective approach.

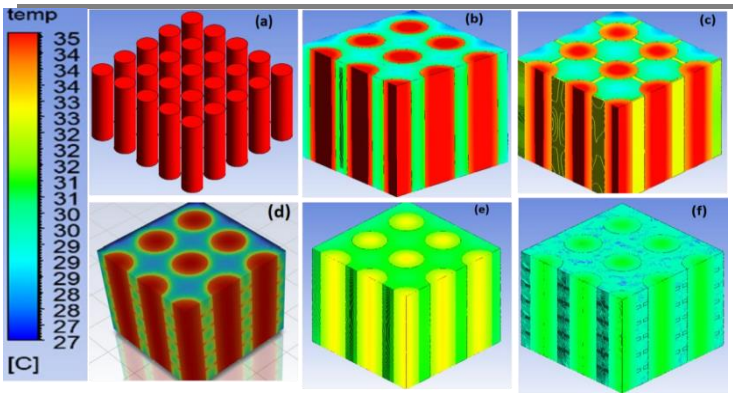

Figure 15 Comparison of temperature distribution for all cases on a common temperature scale

PCM Temperature and Liquid fraction

Fig. 17 shows the temperature rise with time of the phase change material for the case of PCM with additive, which is the case with the maximum temperature inside the optimum range. The graph presents a clear visualization of how the temperature of PCM varies over time. The temperature remains almost constant after reaching the phase change temperature during the phase transition of PCM, indicating that the PCM is effectively absorbing the excess heat generated by the batteries. On the other hand, Fig. 18 indicates the liquid fraction distribution of PCM, showing that the liquid fraction is less than 1 and close to 0.5. This means that the PCM does not melt completely and instead undergoes a partial phase change, indicating the effectiveness of the PCM in absorbing the heat generated by the batteries while maintaining a stable temperature range.

Together, Fig. 16 and 17 provide valuable insights into the effectiveness of PCM with additives in managing the temperature of batteries, making it an optimal cooling mechanism for battery systems.

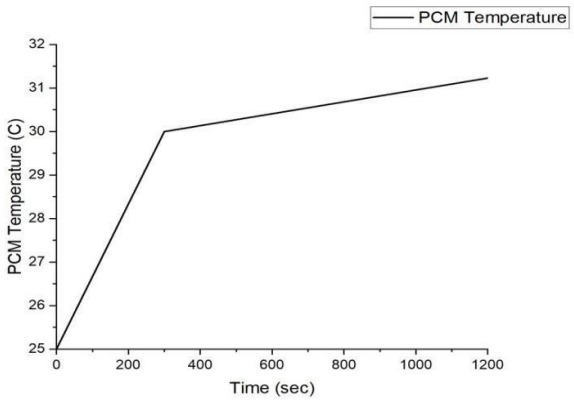

Figure 16 Temperature rise of PCM

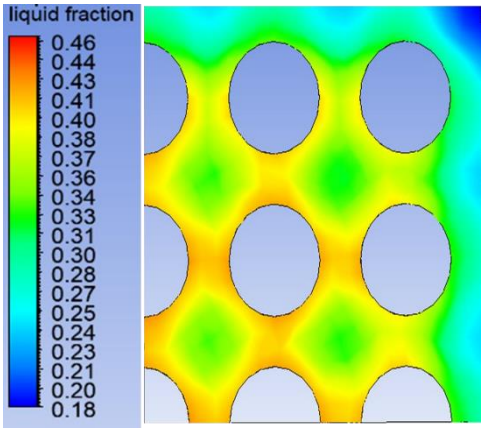

Figure 17 Liquid fraction distribution of PCM

ISSN No. 2454-6194 | DOI: 10.51584/IJRIAS |Volume X Issue VI June 2025

Performance comparison of different fins:

After analyzing common rectangular and circular fins, another uncommon type of fins with spiral shape is considered. The utilization of spiral fins in thermal management analysis presents an intriguing approach due to their unique and complex geometry. Spiral fins with a thickness of 1 mm were carefully analyzed in this study to assess their performance in temperature control for lithium-ion batteries in electric vehicles. The detailed geometry of the model with spiral fins of 1 mm thickness is shown in Figure 19, illustrating the intricate arrangement of the fins. The temperature distribution was then simulated under a 3C discharge rate for a duration of 1200s, and the results were visualized in Figure 20. Remarkably, the maximum temperature recorded was only 34.6°C, which is significantly lower compared to circular fins. This suggests that the use of spiral fins with a thickness of 1 mm could effectively mitigate temperature rise in the battery system, contributing to improved thermal management.

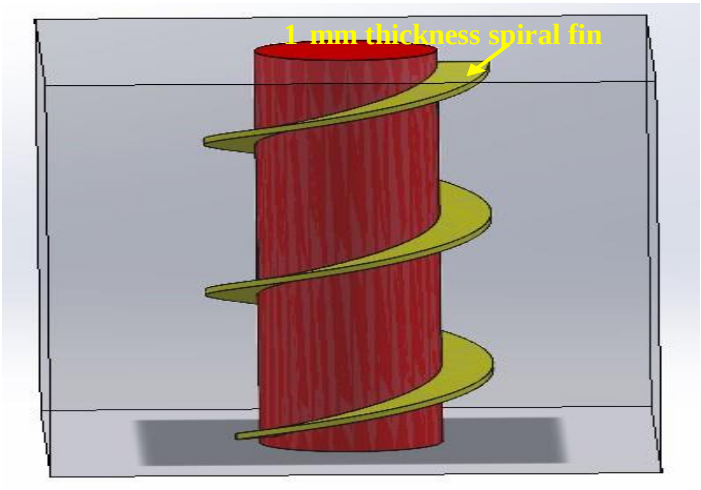

Figure 18 Geometry of spiral fin with 1 mm thickness

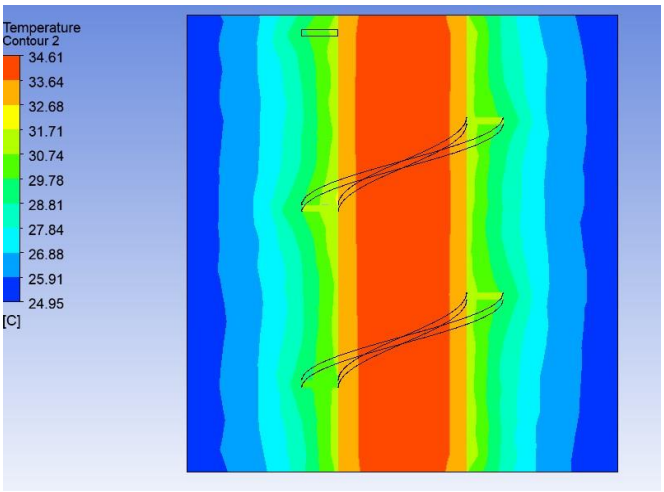

Figure 19 Temperature distribution in case of spiral fins of 1 mm thickness under 3C discharge rate for 1200s

In a similar manner, the performance of spiral fins with a thickness of 2 mm was thoroughly investigated. The geometric configuration of the model with spiral fins of 2 mm thickness is depicted in Figure 21, showcasing the intricate design of the fins. The temperature distribution under a 3C discharge rate for 1200s was visualized in Figure 22, revealing interesting insights. Notably, the maximum temperature recorded was only 34.4°C, which is only 0.5% lower compared to the spiral fins with 1 mm thickness. This suggests that the thickness of the spiral fins may not be an exponential factor in influencing the thermal performance of the model. Similarly, the effect of thickness on the thermal performance of rectangular and circular fins was also found to be minimal, with only minor decreases in maximum temperature observed with increasing thickness.

ISSN No. 2454-6194 | DOI: 10.51584/IJRIAS |Volume X Issue VI June 2025

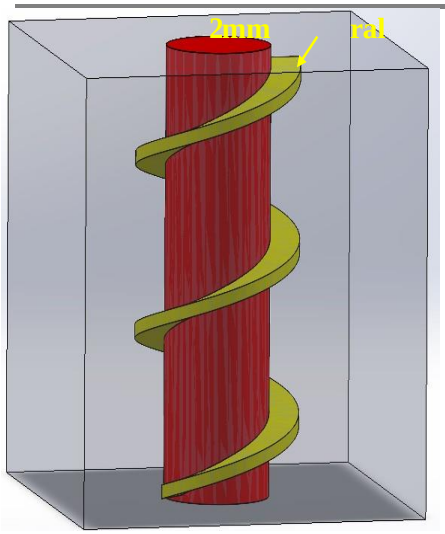

Figure 20 Geometry of spiral fin with 2 mm thickness

To further compare the thermal performance of different fin geometries, a comprehensive analysis was conducted by plotting a graph depicting the rise of maximum temperature with time for rectangular, circular, spiral 1 mm, and spiral 2 mm fins, as shown in Figure 23. The comparison provides valuable insights into the dynamic temperature behavior of different fin designs during battery operation. The results reveal that spiral fins, particularly those with a thickness of 2 mm, demonstrate superior thermal performance compared to circular fins, as they result in lower maximum temperatures. This suggests that the unique geometry of spiral fins could be advantageous in mitigating temperature rise in lithium-ion batteries, potentially contributing to improved battery performance and safety.

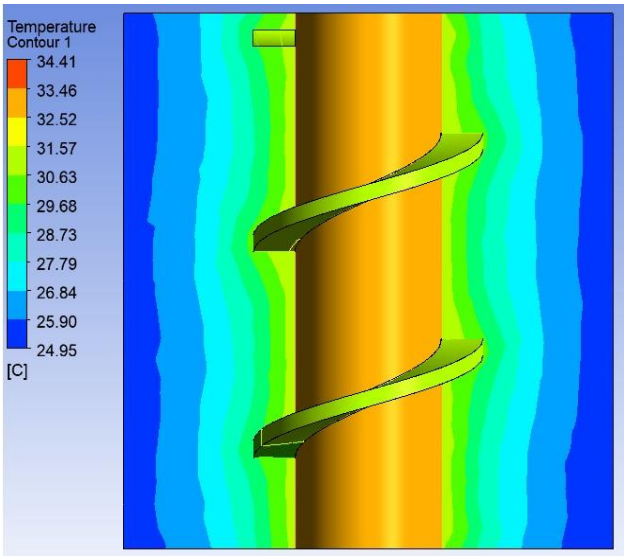

Figure 21 Temperature distribution in case of spiral fins of 2 mm thickness under 3C discharge rate for 1200s

The findings obtained from the analysis of spiral fins with different thicknesses provide valuable information for optimizing battery thermal management system. The results suggest that spiral fins have the potential to effectively dissipate heat and control temperature rise during battery operation, which could contribute to improved battery performance and safety. However, It is worth noting that the complex heat transfer mechanisms and fluid dynamics associated with the unique geometry of spiral fins warrant further investigation. Future research could focus on exploring other spiral fin geometries, as well as their combination with other thermal management techniques, to further enhance the performance and safety of lithium-ion batteries in electric vehicles. In conclusion, the analysis of spiral fins presents a promising approach for thermal management in lithium-ion batteries, and further research in this area could significantly contribute to advancing the BTMS field of study.

ISSN No. 2454-6194 | DOI: 10.51584/IJRIAS |Volume X Issue VI June 2025

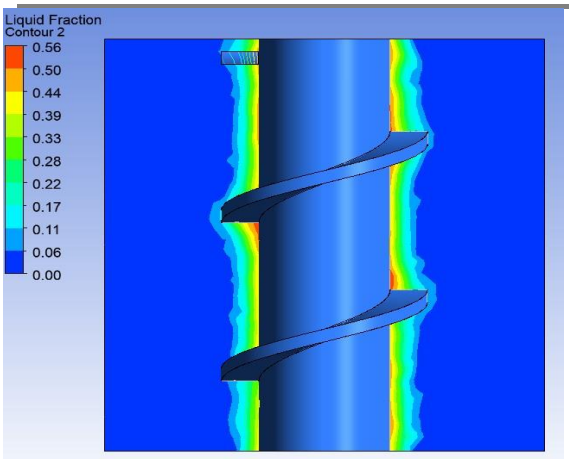

Figure 22 Liquid fraction distribution in case of spiral fins with 2 mm thickness

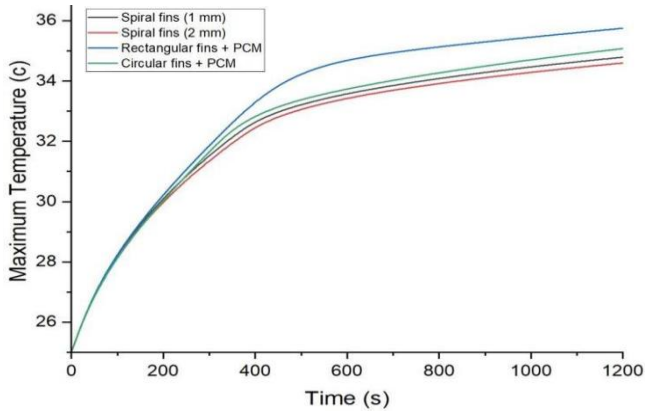

Figure 23 Comparison of maximum temperature rise over time for different fin types

Performance comparison of different additives:

The first set of additives investigated in this study were graphene and carbon nanotubes. The temperature and liquid fraction distributions for PCM with graphene and carbon nanotubes additives are shown in Figure 24. The maximum temperature recorded for this PCM with additives was 34.7 degrees Celsius, and the liquid fraction reached 0.7. This high liquid fraction suggests that the PCM with graphene and carbon nanotubes additives could potentially melt completely under higher discharge rates of 5C or continuous cycles of 3C discharge. Furthermore, the addition of these additives resulted in a decrease in temperature from 36 degrees Celsius (in the case of PCM without any additives) to 34.7 degrees Celsius, indicating their potential for improving the thermal performance of the PCM.

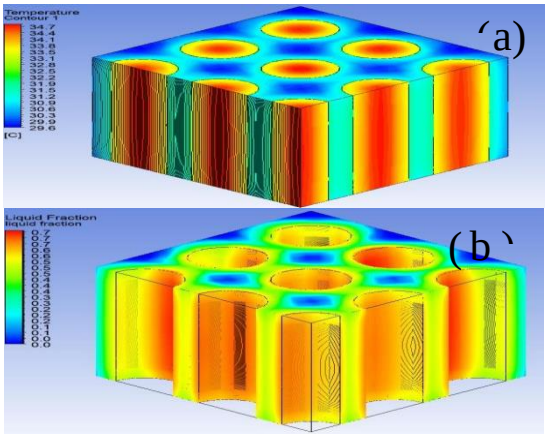

Figure 24 Temperature distribution (a) and Liquid fraction distribution (b) in case of graphene, carbon nanotubes additives

ISSN No. 2454-6194 | DOI: 10.51584/IJRIAS |Volume X Issue VI June 2025

Another set of additives investigated were metal nanoparticles, including Cu, Fe2O3, and Ag. The temperature and liquid fraction distributions for PCM with these metal nanoparticles additives are shown in Figure 25. The maximum temperature recorded for this PCM was 34 degrees Celsius, and the liquid fraction reached 0.6. It was observed that the addition of these metal nanoparticles increased the thermal conductivity of the paraffin PCM to a greater extent compared to graphene and carbon nanotubes additives. This resulted in a decrease in temperature from 36 degrees Celsius (in the case of PCM without any additives) to 34 degrees Celsius, indicating their potential for enhancing the thermal performance of the PCM.

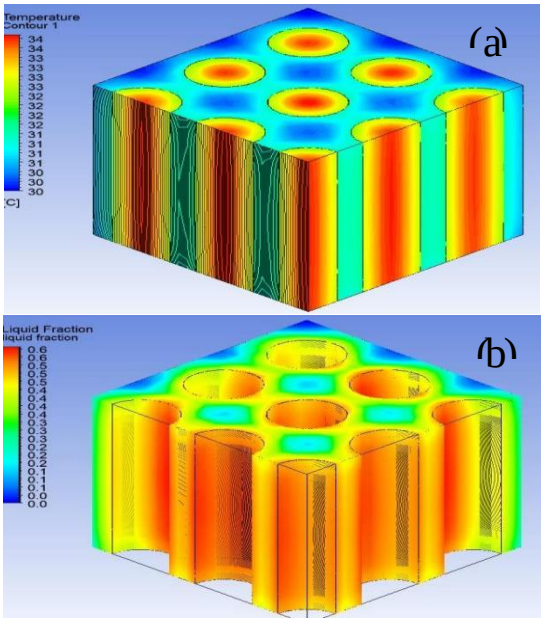

Figure 25 Temperature distribution (a) and Liquid fraction distribution (b) in case of Metal nanoparticles (Cu, Fe2O3, Ag)

The expanded graphite additive has already been analyzed and presented previously. The last set of additives investigated in this study was copper micro fibrous. The temperature and liquid fraction distributions for PCM with copper micro fibrous additives are shown in Figure 27. The maximum temperature recorded for this PCM was 32.9 degrees Celsius, and the liquid fraction reached 0.4. Remarkably, copper micro fibrous additives demonstrated the highest increase in thermal conductivity among all the additives studied. The addition of copper micro fibrous resulted in a significant decrease in temperature from 36 degrees Celsius (in the case of PCM without any additives) to 32.9 degrees Celsius, indicating its remarkable potential for enhancing the thermal performance of the PCM.

In conclusion, the performance of different additives in paraffin-based phase change materials (PCMs) was investigated in this study. Graphene and carbon nanotubes additives showed a moderate decrease in maximum temperature (34.7°C) with a high liquid fraction (0.7), indicating their potential for effective heat dissipation under high discharge rates or continuous cycling. Metal nanoparticles additives, including Cu, Fe2O3, and Ag, demonstrated a higher reduction in maximum temperature (34°C) and increased the thermal conductivity of paraffin PCM to 1 W/mK, indicating their superior thermal enhancement capability.

Furthermore, expanded graphite additives significantly increased the thermal conductivity of paraffin to 5 W/mK, resulting in a maximum temperature of 33.4°C and a liquid fraction of 0.4. Interestingly, copper micro fibrous additives exhibited an astonishing increase in thermal conductivity to 55 W/mK, which is significantly higher than other additives. However, despite its significantly higher thermal conductivity, the performance of copper micro fibrous additives in terms of maximum temperature (32.9°C) and liquid fraction (0.4) was comparable to that of expanded graphite additives with a thermal conductivity of 5 W/mK.

These findings highlight the importance of carefully selecting and optimizing additives for PCM applications based on specific requirements. While additives such as graphene, carbon nanotubes, and metal nanoparticles

ISSN No. 2454-6194 | DOI: 10.51584/IJRIAS |Volume X Issue VI June 2025

may be suitable for applications that demand higher liquid fractions, expanded graphite and copper micro fibrous additives may offer better performance in terms of thermal conductivity.

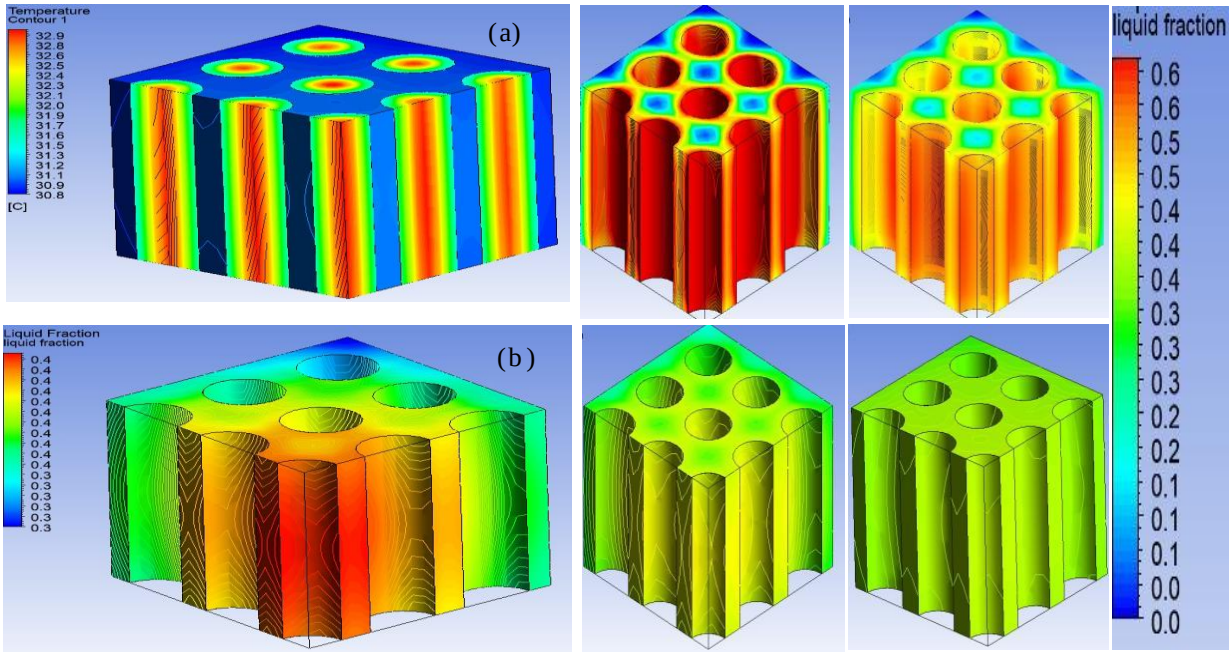

Figure 26 Temperature distribution (a) and Liquid fraction distribution (b) in case of copper micro fibrous

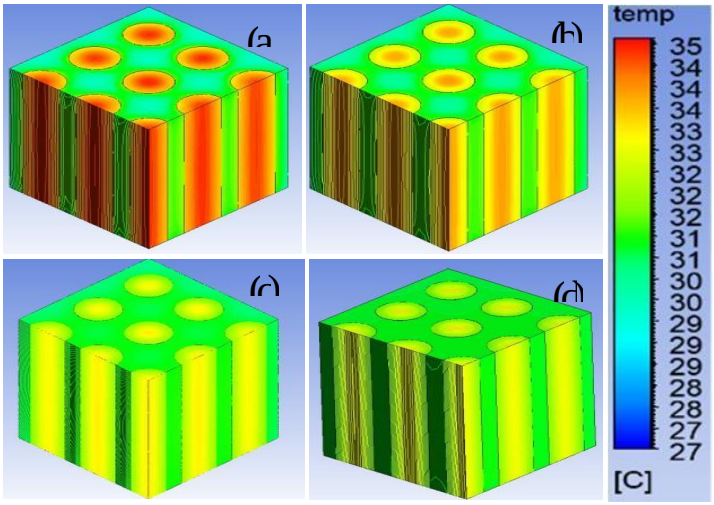

Figure 27 Temperature distribution comparison between additives of a) Graphene and carbon nanotubes b) Metal nanoparticles (Cu, Fe2O3, and Ag) **c)** Expanded graphite and **d)** Copper micro fibrous on common temperature scale

Figure 27 presents a comparison of temperature distributions among different additives on a common scale. It provides a visual representation of the temperature profiles of paraffin-based PCMs with graphene, carbon nanotubes, metal nanoparticles (Cu, Fe2O3, Ag), expanded graphite, and copper micro fibrous additives. Figure 28 illustrates the liquid fraction distribution comparison among these additives on a common scale, showing the variation in the amount of liquid phase present in the PCM at different temperatures. Finally, Figure 29 depicts the temperature rise comparison, highlighting the additives performance with respect to reducing the PCM maximum temperature.

Upon analyzing these figures, it can be observed that the performance of expanded graphite and copper micro fibrous additives is comparable when it comes to maximum temperature reduction and liquid fraction distribution. Both additives exhibit similar trends in temperature rise, indicating that their thermal enhancement capabilities are similar. This suggests that despite the significant difference in thermal conductivity between expanded graphite (5 W/mK) and copper micro fibrous on their overall performance in terms of temperature

ISSN No. 2454-6194 | DOI: 10.51584/IJRIAS |Volume X Issue VI June 2025

reduction and liquid fraction distribution is not significantly different. This finding may have practical implications in selecting suitable additives for PCM-based thermal energy storage systems, considering the cost and availability of different additives

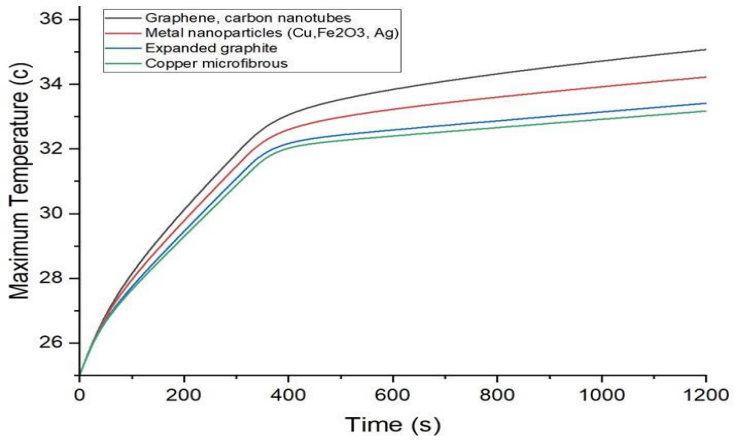

.

Figure 29 Comparison of maximum temperature rise over time for different fin types

FURTHER RESULTS

In the further results of our study, we investigated the effect of increasing thermal conductivity on BTMS performance under a 3C discharge rate for 1200 seconds. As we observed that the performance of copper micro fibrous with a thermal conductivity of 55 W/mK was not significantly different from that of expanded graphite with a thermal conductivity of 5 W/mK, we aimed to understand the relationship between thermal conductivity and maximum temperature in more detail. The results are presented in Figure 31, which shows a clear trend.

From Figure 31, it can be observed that when the initial thermal conductivity of paraffin is low, the influence of thermal conductivity on the maximum temperature of BTMS is more significant. As the thermal conductivity of paraffin increases, the effect of further increasing thermal conductivity on BTMS performance reduces. This is evident from the graph approaching a horizontal line after a thermal conductivity of 3 W/mK. This suggests that the impact of thermal conductivity on the performance of BTMS diminishes as the thermal conductivity of the base material (paraffin) increases, indicating that other factors may become more dominant in influencing the system's behavior at higher thermal conductivities.

These findings highlight the significance of the initial thermal conductivity of the base material in determining the effect of additional thermal conductivity enhancement through additives on the performance of BTMS. It suggests that careful consideration should be given to the selection of additives based on the initial thermal conductivity of the base material in order to achieve optimal performance in PCM-based thermal energy st orage systems.

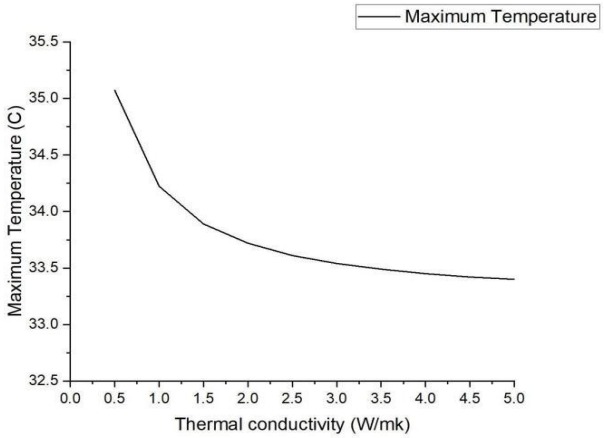

Figure 30 Effect of thermal conductivity on maximum temperature of BTMS

ISSN No. 2454-6194 | DOI: 10.51584/IJRIAS |Volume X Issue VI June 2025

Performing curve fitting on the trend line presented in Figure 30, we obtained Equation 6, which predicts the maximum temperature of paraffin PCM based on its thermal conductivity. The coefficient of determination (R-squared value) for the fitted equation is 0.98, indicating an excellent fit to the data. This high R-squared value suggests that the predicted maximum temperature based on thermal conductivity is highly correlated with the actual maximum temperature observed in our experiments, indicating the reliability of the fitted equation.

$$\boldsymbol{y = -0.0069\,x^3 + 0.1467\,x^2 - 1.0268\,x + 35.877} \quad (6)$$

The high R-squared value of 0.98 indicates that approximately 98% of the variation in the maximum temperature of BTMS can be explained by the thermal conductivity of the base material (paraffin). This equation provides a valuable tool for predicting the maximum temperature of BTMS based on the thermal conductivity of the paraffin PCM, which can be useful in designing and optimizing PCM-based thermal energy storage systems for various applications. Further validation of this equation with additional experimental data and sensitivity analysis could provide more insights into the relationship between thermal conductivity and maximum temperature in PCM-based systems.

CONCLUSIONS AND FUTURE WORK

The present study aimed to investigate the effect of phase change materials (PCM) with various configurations on the temperature control of batteries. The simulations were conducted using computational fluid dynamics (CFD) and validated with experimental data, yielding important findings:

1. PCM significantly reduced and maintained the temperature below 37°C during the full discharge of batteries at 3C rate in 1200s. This demonstrates that PCM is an efficient way for controlling batteries temperature during operation, which is crucial for their safe functioning.

2. Changing the thermal conductivity of PCM from 0.2 W/mK to 5 W/mK using additives improved its performance more than compared to introducing fins. This suggests that additives can be employed to improve PCM's thermal conductivity, which is a critical parameter for increasing its performance.

3. Spiral fins were found to be more effective than circular and rectangular fins in improving the performance of PCM. This indicates that the geometry of fins plays a significant role in enhancing the thermal conductivity of PCM. However, spiral fins are a specific type of fin geometry that may not be commonly used or readily applicable in all situations.

4. Copper micro fibrous and expanded graphite showed the highest increase in thermal performance or reduction in the maximum temperature of the PCM. Metal nanoparticles, including Cu, Fe2O3, and Ag, demonstrated intermediate improvements in thermal performance, followed by graphene and carbon nanotubes. These findings highlight the potential of copper micro fibrous, expanded graphite, and metal nanoparticles as effective additives for enhancing the thermal conductivity and performance of PCM in battery thermal management applications.

5. Comparison of the performance of different additives and fin configurations revealed that there may be an optimal thermal conductivity level for achieving the best performance of the PCM. For example, copper micro fibrous with a thermal conductivity of 55 W/mK and expanded graphite with a thermal conductivity of 5 W/mK showed similar thermal performance. While higher thermal conductivity additives and fins generally resulted in better performance in terms of maximum temperature reduction, there were diminishing returns observed with excessively high thermal conductivity levels. It should be noted that other factors, such as the low radial thermal conductivity of the battery, may become a constraint or bottleneck in achieving further performance improvements through large increases in thermal conductivity.

6. The study also investigated the combined effects of additives and fins on the performance of the PCM. It was found that the use of both additives and fins resulted in a synergistic effect, leading to even lower maximum temperatures compared to using either additives or fins alone. This suggests that the

combination of additives and fins can offer enhanced performance in terms of thermal energy storage, making it a promising approach for optimizing PCM-based systems.

7. Another important finding from this study was that PCM melting did not pose a problem, as the liquid fraction remained below 0.6. This indicates that the PCM can be used without the risk of melting and causing damage to the batteries. This finding is significant for battery safety. The application of PCM as a thermal management solution can effectively mitigate this risk and enhance the safety of battery operation.

8. The summary of performance in case of different configurations is shown in Figure 31 while selecting the optimal fins and additives out of all.

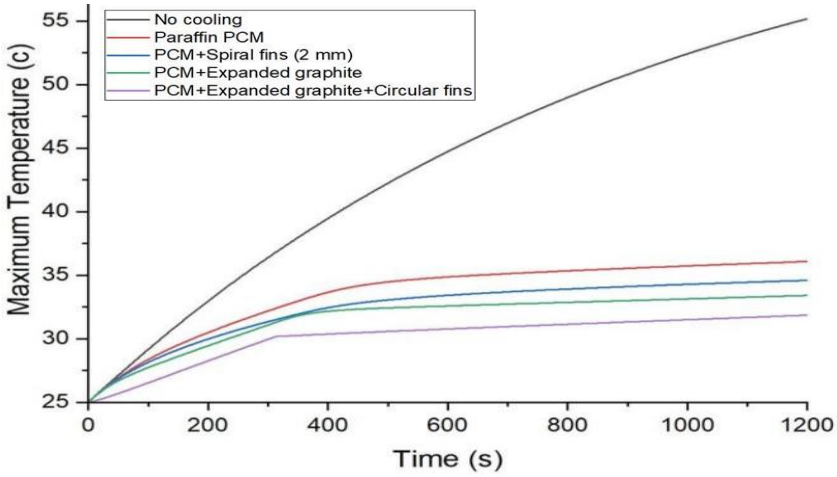

Figure 31 Summary of temperature performance in case of different optimal configurations

In summary, the present study demonstrated the significant effects of additives and fins on the performance of PCM for thermal management of batteries. The optimal thermal conductivity level, fin geometry, and PCM melting behavior were important considerations in designing efficient thermal management systems. The findings of this study contribute to the understanding of PCM based thermal management for batteries and provide a foundation for further research and development in this area.

Further research can be conducted to investigate other types of additives or fin configurations to optimize the performance of PCM for different battery chemistries, operating conditions, and applications. Additionally, the use of hybrid PCM-BTMS can be explored for further improvements in thermal management of batteries. The results of this study have implications for a wide range of applications, including electric vehicles, renewable energy systems, and portable electronic devices, where efficient thermal management of batteries is crucial for their performance, reliability, and safety.

Data Availability Statement:

- The datasets used and analyzed during the current study is available from the corresponding author Muhammad Tahir and novel to this research.

- All data or results generated during this study are included in this published article and are driven from software simulations.

REFERENCES

1. L. Stougie, N. Giustozzi, H. van der Kooi, and A. Stoppato, “Environmental, economic and exergetic sustainability assessment of power generation from fossil and renewable energy sources,” Int J Energy Res, vol. 42, no. 9, pp. 2916–2926, Jul. 2018, doi: 10.1002/er.4037.

2. A. Jokar, B. Rajabloo, M. Désilets, and M. Lacroix, "Review of simplified Pseudo-twoDimensional models of lithium-ion batteries," J Power Sources, vol. 327, pp. 44–55, Sep. 2016, doi: 10.1016/j.jpowsour.2016.07.036.
3. A. Mitra, R. Kumar, D. K. Singh, and Z. Said, "Advances in the improvement of thermalconductivity of phase change material-based lithium-ion battery thermal management systems: An updated review," J Energy Storage, vol. 53, p. 105195, Sep. 2022, doi: 10.1016/j.est.2022.105195.
4. Hannah Ritchie, "Cars, planes, trains: where do CO2 emissions from transport come from?," ourworldindata.org, Oct. 06, 2020.
5. Z. G. Shen, S. Chen, X. Liu, and B. Chen, "A review on thermal management performance enhancement of phase change materials for vehicle lithium-ion batteries," Renewable and Sustainable Energy Reviews, vol. 148. Elsevier Ltd, Sep. 01, 2021. doi: 10.1016/j.rser.2021.111301.
6. M. Malik, I. Dincer, and M. A. Rosen, "Review on use of phase change materials in battery thermal management for electric and hybrid electric vehicles," Int J Energy Res, vol. 40, no. 8, pp. 1011–1031, Jun. 2016, doi: 10.1002/er.3496.
7. A. Jokar, B. Rajabloo, M. Désilets, and M. Lacroix, "Review of simplified Pseudo-twoDimensional models of lithium-ion batteries," Journal of Power Sources, vol. 327. Elsevier B.V., pp. 44–55, Sep. 30, 2016. doi: 10.1016/j.jpowsour.2016.07.036.
8. B. Lin and W. Wu, "The impact of electric vehicle penetration: A recursive dynamic CGE analysis of China," Energy Econ, vol. 94, p. 105086, Feb. 2021, doi: 10.1016/j.eneco.2020.105086.
9. A. Jarrett and I. Y. Kim, "Design optimization of electric vehicle battery cooling plates for thermal performance," J Power Sources, vol. 196, no. 23, pp. 10359–10368, Dec. 2011, doi: 10.1016/j.jpowsour.2011.06.090.
10. P. R. Tete, M. M. Gupta, and S. S. Joshi, "Numerical investigation on thermal characteristics of a liquid-cooled lithium-ion battery pack with cylindrical cell casings and a square duct," J Energy Storage, vol. 48, Apr. 2022, doi: 10.1016/j.est.2022.104041.
11. Y. Huang et al., "Study on the thermal interaction and heat dissipation of cylindrical Lithium-Ion Battery cells," in Energy Procedia, Elsevier Ltd, 2017, pp. 4029–4036. doi: 10.1016/j.egypro.2017.12.321.
12. A. Wazeer, A. Das, C. Abeykoon, A. Sinha, and A. Karmakar, "Phase change materials for battery thermal management of electric and hybrid vehicles: A review," Energy Nexus, vol. 7, p. 100131, Sep. 2022, doi: 10.1016/j.nexus.2022.100131.
13. M. Kiani, S. Omiddezyani, E. Houshfar, S. R. Miremadi, M. Ashjaee, and A. Mahdavi Nejad, "Lithium-ion battery thermal management system with Al2O3/AgO/CuO nanofluids and phase change material," Appl Therm Eng, vol. 180, p. 115840, Nov. 2020, doi: 10.1016/j.applthermaleng.2020.115840.
14. Y. Wei and M. Agelin-Chaab, "Experimental investigation of a novel hybrid cooling method for lithium-ion batteries," Appl Therm Eng, vol. 136, pp. 375–387, May 2018, doi: 10.1016/j.applthermaleng.2018.03.024.
15. A. A. H. Akinlabi and D. Solyali, "Configuration, design, and optimization of air-cooled battery thermal management system for electric vehicles: A review," Renewable and Sustainable Energy Reviews, vol. 125, p. 109815, Jun. 2020, doi: 10.1016/j.rser.2020.109815.
16. Y. Wang, Q. Gao, G. Wang, P. Lu, M. Zhao, and W. Bao, "A review on research status and key technologies of battery thermal management and its enhanced safety," Int J Energy Res, vol. 42, no. 13, pp. 4008–4033, Oct. 2018, doi: 10.1002/er.4158.
17. Z. Y. Jiang and Z. G. Qu, "Lithium–ion battery thermal management using heat pipe and phase change material during discharge–charge cycle: A comprehensive numerical study," Appl Energy, vol. 242, pp. 378–392, May 2019, doi: 10.1016/j.apenergy.2019.03.043.
18. Z. Ling, J. Cao, W. Zhang, Z. Zhang, X. Fang, and X. Gao, "Compact liquid cooling strategy with phase change materials for Li-ion batteries optimized using response surface methodology," Appl Energy, vol. 228, pp. 777–788, Oct. 2018, doi: 10.1016/j.apenergy.2018.06.143.
19. Y. Wang, Z. Wang, H. Min, H. Li, and Q. Li, "Performance investigation of a passive battery thermal management system applied with phase change material," J Energy Storage, vol. 35, p. 102279, Mar. 2021, doi: 10.1016/j.est.2021.102279.
20. M. Al-Zareer, I. Dincer, and M. A. Rosen, "A review of novel thermal management systems for batteries," Int J Energy Res, vol. 42, no. 10, pp. 3182–3205, Aug. 2018, doi: 10.1002/er.4095.

21. W. Wu, S. Wang, W. Wu, K. Chen, S. Hong, and Y. Lai, "A critical review of battery thermal performance and liquid based battery thermal management," Energy Convers Manag, vol. 182, pp. 262–281, Feb. 2019, doi: 10.1016/j.enconman.2018.12.051.
22. P. Huang, A. Verma, D. J. Robles, Q. Wang, P. Mukherjee, and J. Sun, "Probing the cooling effectiveness of phase change materials on lithium-ion battery thermal response under overcharge condition," Appl Therm Eng, vol. 132, pp. 521–530, Mar. 2018, doi: 10.1016/j.applthermaleng.2017.12.121.
23. W. Wu, G. Zhang, X. Ke, X. Yang, Z. Wang, and C. Liu, "Preparation and thermal conductivity enhancement of composite phase change materials for electronic thermal management," Energy Convers Manag, vol. 101, pp. 278–284, Sep. 2015, doi: 10.1016/j.enconman.2015.05.050.
24. Z. Wang, Z. Zhang, L. Jia, and L. Yang, "Paraffin and paraffin/aluminum foam composite phase change material heat storage experimental study based on thermal management of Liion battery," Appl Therm Eng, vol. 78, pp. 428–436, Mar. 2015, doi: 10.1016/j.applthermaleng.2015.01.009.
25. M. Alipanah and X. Li, "Numerical studies of lithium-ion battery thermal management systems using phase change materials and metal foams," Int J Heat Mass Transf, vol. 102, pp. 1159–1168, Nov. 2016, doi: 10.1016/j.ijheatmasstransfer.2016.07.010.
26. A. Hussain, C. Y. Tso, and C. Y. H. Chao, "Experimental investigation of a passive thermal management system for high-powered lithium ion batteries using nickel foam-paraffin composite," Energy, vol. 115, pp. 209–218, Nov. 2016, doi: 10.1016/j.energy.2016.09.008.
27. A. Hussain, I. H. Abidi, C. Y. Tso, K. C. Chan, Z. Luo, and C. Y. H. Chao, "Thermal management of lithium ion batteries using graphene coated nickel foam saturated with phase change materials," International Journal of Thermal Sciences, vol. 124, pp. 23–35, Feb. 2018, doi: 10.1016/j.ijthermalsci.2017.09.019.
28. M. Mehrabi-Kermani, E. Houshfar, and M. Ashjaee, "A novel hybrid thermal management for Li-ion batteries using phase change materials embedded in copper foams combined with forced-air convection," International Journal of Thermal Sciences, vol. 141, pp. 47–61, Jul. 2019, doi: 10.1016/j.ijthermalsci.2019.03.026.
29. J. He, X. Yang, and G. Zhang, "A phase change material with enhanced thermal conductivity and secondary heat dissipation capability by introducing a binary thermal conductive skeleton for battery thermal management," Appl Therm Eng, vol. 148, pp. 984– 991, Feb. 2019, doi: 10.1016/j.applthermaleng.2018.11.100.
30. W. H. Zhu, H. Yang, K. Webb, T. Barron, P. Dimick, and B. J. Tatarchuk, "A novel cooling structure with a matrix block of microfibrous media / phase change materials for heat transfer enhancement in high power Li-ion battery packs," J Clean Prod, vol. 210, pp. 542– 551, Feb. 2019, doi: 10.1016/j.jclepro.2018.11.043.
31. G. Jiang, J. Huang, Y. Fu, M. Cao, and M. Liu, "Thermal optimization of composite phase change material/expanded graphite for Li-ion battery thermal management," Appl Therm Eng, vol. 108, pp. 1119–1125, Sep. 2016, doi: 10.1016/j.applthermaleng.2016.07.197.
32. Y. Azizi and S. M. Sadrameli, "Thermal management of a LiFePO4 battery pack at high temperature environment using a composite of phase change materials and aluminum wire mesh plates," Energy Convers Manag, vol. 128, pp. 294–302, Nov. 2016, doi: 10.1016/j.enconman.2016.09.081.
33. W. Situ et al., "A thermal management system for rectangular LiFePO4 battery module using novel double copper mesh-enhanced phase change material plates," Energy, vol. 141, pp. 613–623, Dec. 2017, doi: 10.1016/j.energy.2017.09.083.
34. G. Karimi, M. Azizi, and A. Babapoor, "Experimental study of a cylindrical lithium ion battery thermal management using phase change material composites," J Energy Storage, vol. 8, pp. 168–174, Nov. 2016, doi: 10.1016/j.est.2016.08.005.
35. D. Zou et al., "Preparation of a novel composite phase change material (PCM) and its locally enhanced heat transfer for power battery module," Energy Convers Manag, vol. 180, pp. 1196–1202, Jan. 2019, doi: 10.1016/j.enconman.2018.11.064.
36. M. Alipanah and X. Li, "Numerical studies of lithium-ion battery thermal management systems using phase change materials and metal foams," Int J Heat Mass Transf, vol. 102, pp. 1159–1168, Nov. 2016, doi: 10.1016/j.ijheatmasstransfer.2016.07.010.

37. J. Zhang et al., "Experimental investigation of the flame retardant and form-stable composite phase change materials for a power battery thermal management system," J Power Sources, vol. 480, p. 229116, Dec. 2020, doi: 10.1016/j.jpowsour.2020.229116.
38. P. Ping, R. Peng, D. Kong, G. Chen, and J. Wen, "Investigation on thermal management performance of PCM-fin structure for Li-ion battery module in high-temperature environment," Energy Convers Manag, vol. 176, pp. 131–146, Nov. 2018, doi: 10.1016/j.enconman.2018.09.025.
39. Z. Wang, H. Zhang, and X. Xia, "Experimental investigation on the thermal behavior of cylindrical battery with composite paraffin and fin structure," Int J Heat Mass Transf, vol. 109, pp. 958–970, Jun. 2017, doi: 10.1016/j.ijheatmasstransfer.2017.02.057.
40. Z. Sun, R. Fan, F. Yan, T. Zhou, and N. Zheng, "Thermal management of the lithium-ion battery by the composite PCM-Fin structures," Int J Heat Mass Transf, vol. 145, p. 118739, Dec. 2019, doi: 10.1016/j.ijheatmasstransfer.2019.118739.
41. N. Zheng, R. Fan, Z. Sun, and T. Zhou, "Thermal management performance of a finenhanced phase change material system for the lithium-ion battery," Int J Energy Res, vol. 44, no. 9, pp. 7617–7629, Jul. 2020, doi: 10.1002/er.5494.
42. J. Weng, Y. He, D. Ouyang, X. Yang, G. Zhang, and J. Wang, "Thermal performance of PCM and branch-structured fins for cylindrical power battery in a high-temperature environment," Energy Convers Manag, vol. 200, p. 112106, Nov. 2019, doi: 10.1016/j.enconman.2019.112106.
43. V. G. Choudhari, A. S. Dhoble, and S. Panchal, "Numerical analysis of different fin structures in phase change material module for battery thermal management system and its optimization," Int J Heat Mass Transf, vol. 163, p. 120434, Dec. 2020, doi: 10.1016/j.ijheatmasstransfer.2020.120434.
44. D. Kong, R. Peng, P. Ping, J. Du, G. Chen, and J. Wen, "A novel battery thermal management system coupling with PCM and optimized controllable liquid cooling for different ambient temperatures," Energy Convers Manag, vol. 204, Jan. 2020, doi: 10.1016/j.enconman.2019.112280.